HHS Public Access

Author manuscript

Mol Imaging Biol. Author manuscript; available in PMC 2020 November 04.

Published in final edited form as:

Mol Imaging Biol. 2014 October ; 16(5): 739–746. doi:10.1007/s11307-014-0730-7.

Biodistribution and Radiation Dosimetry of the Carbonic Anhydrase IX Imaging Agent [^{18}F]VM4–037 determined from PET/CT Scans in Healthy Volunteers

Mohan Doss[1], **Hartmuth C. Kolb**[2], **Joseph C. Walsh**[2], **Vani P. Mocharla**[2], **Zhihong Zhu**[3], **Michael Haka**[3], **R. Katherine Alpaugh**[4], **David Y.T. Chen**[5], **Jian Q. Yu**[1]

[1]Diagnostic Imaging, Fox Chase Cancer Center, Philadelphia, PA

[2]Biomarker Research, Siemens Molecular Imaging Inc., Culver City, CA

[3]Biomarker Research, Siemens Molecular Imaging Inc., North Wales, PA

[4]Protocol Lab, Fox Chase Cancer Center, Philadelphia, PA

[5]Department of Surgery, Fox Chase Cancer Center, Philadelphia, PA

Abstract

Purpose: [^{18}F]VM4–037 has been developed as a positron emission tomography (PET) imaging marker to detect carbonic anhydrase IX (CA-IX) over-expression and is being investigated for use as a surrogate marker for tissue hypoxia. The purpose of this study was to determine the biodistribution and estimate the radiation dose from [^{18}F]VM4–037 using whole body PET/CT scans in healthy human volunteers.

Procedures: Successive whole body PET/CT scans were performed after intravenous injection of [^{18}F]VM4–037 in four healthy humans. The radiotracer uptakes in different organs were determined from the analysis of the PET scans. Human radiation doses were estimated using OLINDA/EXM software.

Results: High uptake of [^{18}F]VM4–037 was observed in liver and kidneys, with little clearance of activity during the study period, with mean standardized uptake values of ~35 in liver and ~22 in kidneys at ~1 hr after injection. The estimated effective dose was 28±1 μSv/MBq and the absorbed doses for the kidneys and liver were 273±31 and 240±68 μGy/MBq respectively, for the adult male phantom. Hence, the effective dose would be 10±0.5 mSv for the anticipated injected activity of 370 MBq, and kidney and liver doses would be 101±11 and 89±25 mGy, respectively.

Conclusions: [^{18}F]VM4–037 displayed very high uptake in liver and kidneys with little clearance of activity during the study period, resulting in these organs receiving the highest radiation doses among all bodily organs. Though the effective dose and the organ doses are within

Corresponding Author: Jian Q. Yu, Diagnostic Imaging, Fox Chase Cancer Center, 333 Cottman Avenue, Philadelphia, PA 19111-2497. Phone: 215 728-3865, Fax: 215 728-4755, Michael.Yu@fccc.edu.

Conflict of Interest Statement

Joseph C. Walsh and Zhihong Zhu are employees of Siemens Molecular Imaging Inc. Hartmuth C. Kolb, Vani P. Mocharla, and Michael Haka were previously employees of Siemens Molecular Imaging Inc. at the time of the work described here. Fox Chase Cancer Center performed the research work described in this paper under a research contract with Siemens Molecular Imaging Inc. None of the authors received any additional compensation for performing this work.

the limits considered as safe, the enhanced uptake of [^{18}F]VM4–037 in kidneys and liver will make the compound unsuitable for imaging over-expression of CA-IX in those two organs. However, the tracer may be suitable for imaging over-expression of CA-IX in lesions in other regions of the body such as in the lungs or head and neck region.

Keywords

^{1}[^{18}F]VM4–037; Biodistribution; Internal Dosimetry; Carbonic Anhydrase IX; PET

Introduction

Carbonic anhydrase IX (CA-IX) is a cell-surface expressed enzyme which catalyzes the reversible transformation between bicarbonate anion and carbon dioxide, a process necessary for regulating cellular pH [1–2]. CA-IX protein is also thought to mediate the regulation of cell proliferation in response to hypoxic conditions and may be involved in ontogenesis, metastasis spread, tumor progression and poor response to therapy [3–5]. Normal CA-IX expression in mammals is typically confined to the gastro-intestinal tract, including the stomach and gallbladder, and is not normally expressed in the majority of bodily organs [2]. The abnormal expression of CA-IX has been detected in many carcinomas originating from CA-IX negative tissues including brain, kidney, lung, breast, uterine, and cervical tissues. The unique over-expression profile makes CA-IX a particularly attractive target for both therapeutics and imaging probes [6].

The ectopic expression of CA-IX is closely linked to both the presence of tumor hypoxia and poor patient outcomes. Physiologically, CA-IX expression becomes elevated at oxygen tensions below 20 mm Hg [7], and on the molecular level, CA-IX expression is responsive to hypoxia inducible factor 1α (HIF1α) transcriptional activation. CA-IX over-expression has also been linked to the tumoral uptake of positron emission tomography (PET) hypoxia imaging agents, [^{18}F]FMISO and [^{18}F]HX4, in head and neck cancer patients [8]. The over-expression of CA-IX is a negative prognostic factor for survival in non-small-cell lung cancer (NSCLC) [9], brain cancer [10], renal cancer [11], breast cancer [12], and cervical cancer [13] and its prognostic significance in head and neck cancer has also been reported [14–15]. In certain tumors, such as renal cell carcinoma, CA-IX expression is not directly related to hypoxia, but rather to a mutation in the Von Hippel Lindau tumor suppressor gene [16].

The development of a wide range of potent and selective CA-IX inhibitors is enabling both targeted diagnostic and therapeutic applications in cancer patients. Several CA-IX targeting monoclonal antibodies have been developed for immunological based therapies [17]. The ability to use radiolabeled CA-IX targeting antibodies for diagnostic purposes has also been reported. Recent clinical PET imaging data have shown that ^{124}I-girentuximab is a feasible imaging agent for detecting malignant clear cell renal cell carcinomas [18]. As an alternative to immunological based approaches, small molecule inhibitors targeting CA-IX have also been extensively developed. Small molecules targeting CA-IX are either coumarin-based suicide inhibitors or sulfonamides that confer their inhibitory activity by binding metals in the CA-IX active site [19–20]. Despite the multiplicity and diversity of developed CA-IX

targeting therapeutics, the development of ligands for CA-IX PET imaging remains scarce. [1][18F]VM4–037 was developed as a small molecule inhibitor of CA-IX utilizing the sulfonamide pharmacophore and is a derivative of the promiscuous CA ligand ethoxzolamide. The free carboxylate of [18F]VM4–037 at physiological pH (pH = 7.4) renders molecule cell membrane impermeable enabling selective targeting of extracellular CA-IX protein while avoiding binding to competing intracellular CA isozymes. The localization of [18F]VM4–037 into tissues over-expressing CA-IX has been previously evaluated pre-clinically [21] warranting further exploration in patients. The main goal of this study was to determine the biodistribution and dosimetry of [18F]VM4–037 in humans using PET.

Materials and methods

Radiopharmaceutical Preparation

(S)-3-(4-(2-[F-18]fluoroethoxy)phenyl)-2-(3-methyl-2-(4-((2-sulfamoylbenzo[d]thiazol-6-yloxy)methyl)-1H-1,2,3-triazol-1-yl)butanamido)propanoicacid, also referred to as [18F]VM4–037 has the chemical structure shown in Fig. 1. Production of [18F]VM4–037 was performed in an automated synthesis module. Cyclotron-produced aqueous [18F]fluoride ion (~78 GBq) was passed through an anion exchange resin cartridge to sequester the [18F]fluoride ion from the target water. The [18F]fluoride was eluted from the ion exchange column into the reaction vessel using a solution of tetrabutylammonium bicarbonate (13 mg) in water (0.6 mL). An aliquot of acetonitrile (0.9 mL) was subsequently added into the reaction vessel. The mixture was dried by heating between 70 to 115°C under a stream of inert gas (Ar) under reduced pressure (250 mbar). After the drying procedure was completed, a solution of VM4–037 precursor 1 (15 mg, 13.4 μmol) dissolved in acetonitrile (0.9 mL) was added to the reaction vessel containing the anhydrous [18F]fluoride ion. The vessel was heated to approximately 85°C for 5–10 minutes. After the reaction was complete, the product was diluted with water (up to 5 mL total volume). The crude reaction mixture was transferred to the HPLC sample loop (5 mL) and purified via semi-preparative HPLC (Phenomenex Gemini C18, 5μ 250 × 10 mm, 5.5 mL/min), using 60% MeCN (containing 0.1% formic acid (v/v) : 40% of 0.1% aqueous formic acid (v/v). The column effluent was monitored using UV (254 nm and radiometric detectors connected in series). While the material was being purified, the reaction vessel was rinsed with acetonitrile (1 mL) to remove residual impurities. The retention time of the 18F-labeled VM intermediate 2 in this system was approximately 16 minutes. The purified fraction eluted from the HPLC purification column was diluted with water (20 mL) and captured onto a C18 SepPak cartridge. The C18 SepPak cartridge was rinsed with acetonitrile (1.0 mL) to release the intermediate back into the reaction vessel. The purified [18F]VM4–037 intermediate was then treated with aqueous lithium hydroxide (0.25N, 0.5 mL) and the mixture stirred at 40°C for 5 minutes. Aqueous hydrochloric acid (4N, 0.4 mL) was then added and the reaction vessel was heated to 70°C for 5 min. The reaction mixture was then cooled and diluted to the HPLC loop volume with 50% aqueous acetonitrile and purified via chromatographic separation using a semi-preparative HPLC column (Phenomonex Gemini, 5μ, C18, 250 × 10 mm) using 34% acetonitrile (containing 0.1% formic acid (v/v), 66% aqueous 0.1% formic acid (v/v) as the eluent, at a flow rate of 5.0 mL/min (see Fig. 2). The purified [18F]VM4–

037 fraction (retention time: 7 minutes) was collected and diluted in 50 mL sterile water for injection. This aqueous solution was passed through a C18 Sep-Pak and washed with an additional 10 mL of sterile water for injection. [^{18}F]VM4–037 was then eluted from C18 Sep-Pak cartridge using dehydrated ethanol, USP (0.5 – 1.0 mL), which was diluted with sterile water (4.5–9.0 mL) to afford a final formulation of [^{18}F]VM4–037 in a maximum of 10% ethanol:water (v/v). The solution was then processed through a 0.22 μm sterile filter into a sterile vial. The average decay-corrected radiochemical yield of [^{18}F]VM4–037 was 8.4±3.9% (n=4), and the average specific activity was 548±246 GBq/μmol (n=4).

Subjects:

Approval for the study was obtained from the Research Review Committee, Institutional Review Board and Radiation Safety Committee of Fox Chase Cancer Center. The trial was registered with Clinicaltrial.gov and given the identified number ClinicalTrials.gov identifier: NCT00884520. Two male and two female healthy volunteers (mean age ± SD, 44±15, range 30–65) were enrolled in the study after obtaining written informed consent. The subjects' weights were 72±10 kg (range, 59–84 kg). The subjects were deemed to be in good health based on their clinical history, physical examination, standard blood and urine tests, and electrocardiogram.

PET/CT Acquisition—The study subjects were administered 584±143 MBq (range 401–728 MBq) of [^{18}F]VM4–037 intravenously while laying on the bed of the PET/CT scanner. Immediately after the injection, five whole body PET/CT scans were performed in quick succession on a Discovery LS PET/CT scanner (GE Healthcare). By using a very low tube current setting for attenuation correction CT scans, we kept the radiation dose to the subjects as low as reasonably achievable. The CT scans were performed in the helical mode at 140 kVp, with rotation time of 0.8 sec, slice thickness of 5 mm, slice interval of 4.25 mm, and the tube current used was 10 mA.

The PET acquisitions were performed in 2-D mode from the vertex of the head to mid-thigh. The five PET scans covered 7 bed positions (with a single slice overlap between the positions), and were started at approximately 11, 59, 87, 112 and 133 minutes after injection. Also, after the first PET scan, a PET/CT scan of mid-thigh to toes was performed. The subjects' blood pressure, temperature, and pulse were measured before the injection of the radiotracer, after the first, second, and final PET scans, and on the following day at about 24 hours after injection time. Electrocardiograms accompanied vitals before the administration of [^{18}F]VM4–037, following the first and second PET/CT scans, and at 24 hrs.

Blood samples for analysis were obtained prior to injection of the tracer and at various time points during PET imaging. High-performance liquid chromatography was used for the plasma metabolite analysis. Whole blood samples were assayed for radioactivity in counts per minute. Separation of plasma from whole blood was accomplished using centrifugation (1,274 x g for 5 minutes) and the weight of separated plasma was recorded. Non-radioactive VM4–037 standard (20 μl of a 0.53 mg/mL in 14% EtOH in PBS (1x strength)) and acetonitrile (400 μL) were added to a sample of plasma (400 μL). After vortexing the sample for 30 seconds and subjecting it to high speed centrifugation (11,388 x g for 8 minutes), the

protein-free plasma was separately weighed and the radioactivity was assayed. The radioactivity of the pellet was also assayed. A sample (100 μl) of the protein-free plasma was analyzed by radioHPLC (Agilent 1100 HPLC system equipped with a Gemini C18 analytical column (5 μm, 150 × 4.6 mm, flow = 1 mL/min) with mobile phase A (water w/ 0.05% trifluoroacetic acid (TFA)) and B (acetonitrile w/ 0.05% TFA) and a UV detector set to 254 nm. Eluent fractions for radioactive analysis were collected from the radioHPLC at 1 minute intervals and individually counted. The percentage of parent to metabolites was extracted from the radioHPLC traces.

Data Analysis—We utilized the ordered subsets expectation maximization iterative reconstruction method with 28 subsets and 2 iterations to generate the PET images for a 50 cm diameter field of view, including corrections for randoms and scatter, and using the CT scan for attenuation correction. Since the first two PET scans covered the whole body from head to toe before the subject voided, integration of the total activity in these two scans and comparison to the administered activity provided a confirmation of activity determined from the PET images.

We used MIMVista software (MimVista Corp, Cleveland, OH) to display the PET images, draw the volume regions of interest (ROIs) for the major organs, and determine the activity in the organs. For the organs well-visualized in the PET scans (brain, gallbladder, liver, stomach, lower and upper large intestines, kidneys, and bladder), ROIs were drawn readily. Since the small intestine could not be clearly identified, its ROI was inferred using the boundaries of the nearby organs. The percentage administered activity (%IA) was then calculated for the individual organs for all the PET images.

Normalized Number of Disintegrations—The %IA for each organ in each of the PET scans was fitted to an exponential (or sum of exponentials) function in OLINDA/EXM (Organ Level Internal Dose Assessment) software [22] to calculate the normalized number of disintegrations, i.e. the total number of disintegrations per unit administered activity. For the remainder of body activity, we used the injected activity minus the activity in all the source organs and in collected urine. The half-times for biological excretion were calculated by fitting the injected activity minus accumulated urine activity to an exponential function of time. To estimate the normalized number of disintegrations in bladder, 1 hr and 4.8 hr bladder voiding models were used. The standardized adult male and female models of the OLINDA/EXM were utilized with the above estimated normalized number of disintegrations in order to calculate the absorbed doses in the different organs.

Results:

For the four subjects in the study, the amount of [^{18}F]VM4–037 activity injected was 584±143 MBq (mean±S.D.). There were no clinically significant effects on the vital signs that were monitored, i.e. blood pressure, temperature, pulse, and electrocardiogram, or in blood tests, during the study period of 2.2 hrs or on the following day’s examination.

The average extraction efficiency of [^{18}F]VM4037 from whole blood was 53.4% (S.D. = 3.6%). The blood-to-plasma ratio of radioactivity was varied from 1:1.1 to 1:1.9 in the 90-

min duration of the metabolism samples. The protein-to-plasma ratio of radioactivity varied from 1:1 to 1.7:1 in the 90-min duration of the metabolism samples. Test of the plasma samples indicated that over 98% of [^{18}F]VM4–037 remained intact in the plasma for 90 minutes after injection. The plasma clearance half-time of [^{18}F]VM4–037 was ~18 minutes.

Figure 3 shows a maximum intensity projection (MIP) image from the PET scans of one of the subjects. Immediately after injection, the liver and kidneys experienced considerable uptake while the urinary bladder had considerably lower uptake of the tracer. None of the other organs could be visualized above the background level. There was little clearance of the liver and kidney activities in later PET images. The standardized uptake values in the liver and kidneys at ~60 minutes after injection averaged to nearly 32 and 23, respectively. Other areas of the body had lower standardized uptake values. Liver uptake in the four subjects was in the range of 32% ID to 54% ID at 11 minutes after injection. The organ with the next highest uptake was kidneys, with the uptake in the range of 14% ID to 17% ID. The total activity in the urine collected during the 2.2 hour period after injection, as estimated from the measurements of urine samples in the well counter, was only ~4% of the injected activity. Fig. 4 shows the decay-corrected percent administered activity for the 3 organs with the highest activities.

Table 1 shows the normalized number of disintegrations for the various organs. Table 2 shows the average doses in the organs. The mean effective doses for the adult male phantom for the 1 h and 4.8 h bladder-voiding models were 26±1 μSv/MBq and 28±1 μSv/MBq, respectively. The adult female phantom doses were ~22% higher. The two organs with the highest radiation absorbed doses were the kidneys and the liver, with doses of 273±31 and 240±68 μGy/MBq respectively. Hence, effective dose for a patient injected with 370 MBq of [^{18}F]VM4–037 would be 10±0.5 mSv, and the doses to kidneys and liver would be 101±11 and 89±25 mGy respectively.

Discussion:

[^{18}F]VM4–037, which has been developed to image CA-IX expression, has been studied in healthy subjects. This study provides information on the background uptake levels in normal organs and also assesses the potential radiation exposure in humans through whole body PET imaging.

[^{18}F]VM4–037 revealed a biodistribution dominated by activity in the liver and kidneys and little renal clearance, with only 4% of injected activity excreted within the 2.2 hour duration of the study. Urinary bladder showed diffuse uptake. There was no evidence of the tracer above background levels in the large intestines during the 2.2 hour imaging period. [^{18}F]VM4–037 was found to be intact in human plasma up to 90 minutes post injection.

The plasma half-life of [^{18}F]VM4–037 was calculated to be 18 minutes, which is similar in magnitude to that of [^{18}F]RGD-K5 (12 minutes) [23]. Because [^{18}F]VM4–037 exhibits a relatively fast plasma clearance profile and low non-specific binding in the muscle, the background signal in patients quickly subsides leaving little residual signal. This clearance

profile provides an opportunity to visualize metastatic disease or primary tumors in the lymph nodes, lung and head and neck region.

The organs that received the highest doses were the kidneys (273±31 μGy/MBq), liver (240±68 μGy/MBq) and gallbladder (63±17 μGy/MBq). Adrenals and pancreas had doses of 31±4 and 26±3 μGy/MBq respectively. The remaining organs had doses in the range of 2 to 17 μGy/MBq. The effective dose for the 1 hr and 4.8 hr bladder-voiding models were 26.2±1.3 μSv/MBQ and 27.8±1.4 μSv/MBQ respectively. Hence, effective dose for a patient injected with 370 MBq of [^{18}F]VM4–037 in the 4.8 hr bladder voiding model would be 10±0.5 mSv, the kidney and liver doses would be 101±11 and 89±25 mGy respectively. The typical patient effective dose is well below the whole body dose limit of 30 mSv specified by FDA for research subjects [24].

Table 3 lists the organ doses for [^{18}F]VM4–037 from the present study and the organ doses for [^{18}F]FDG from [25] for comparison. The absorbed doses in kidneys and liver were much higher for [^{18}F]VM4–037 than [^{18}F]FDG. This uptake profile is consistent with the notion that both naturally occurring metalloenzymes in the liver and organic anion transporters in the kidneys are anticipated to non-specifically bind the sulfonamide and carboxylate moieties present in [^{18}F]VM4–037 [26]. The absorbed doses in the gallbladder and adrenals were higher for [^{18}F]VM4–037 than [^{18}F]FDG consistent with the observed expression patterns of CA-IX in these organs [27–29]. Very little of [^{18}F]VM4–037 (~4% in 2.2 hrs) was excreted through the urinary system as a result of the high retention of the tracer in the kidneys and consequently the urinary bladder had a much lower dose for [^{18}F]VM4–037 as compared to [^{18}F]FDG. The uptake of [^{18}F]VM4–037 was elevated in the stomach wall, a tissue known for expressing elevated levels of CA-IX. Conversely, we observed that the spleen had a relatively low uptake of the tracer relative to [^{18}F]FDG which is compatible with the subdued levels of CA-IX noted in spleen tissue [29]. The overall uptake of [^{18}F]VM4–037 in the brain was low relative to [^{18}F]FDG as the polar carboxylate and triazole functional groups in [^{18}F]VM4–037 hinder the tracer from appreciably crossing the blood-brain barrier. For the remaining organs, the calculated organ doses for [^{18}F]VM4–037 were similar to the [^{18}F]FDG.

The biodistribution profile of [^{18}F]VM4–037 in healthy volunteers provides some insight into the possible PET imaging applications of [^{18}F]VM4–037. From the PET images, the retention of [^{18}F]VM4–037 in both the kidneys and liver is considerably higher than other ^{18}F-labeled PET compounds which may hamper imaging CA-IX over-expression in cancer patients with clear cell renal cell or hepatic carcinomas [30]. Even though the background signal is high, if the tumor accumulates more tracer than the background, it could still be detected. Further studies with cancer patients are warranted to clarify this. For other regions, the rapid plasma clearance and low background signal of [^{18}F]VM4–037 in the muscle may enable detecting metastatic spread into lymph nodes that over-express CA-IX or even primary lung, breast or and head and neck cancers, which are known to over-express CA-IX [31–34]. As mentioned previously, the overall uptake of [^{18}F]VM4–037 into the human brain is low, which would normally preclude using this tracer for brain imaging studies. However, glioblastoma patients are reported to have disrupted blood brain barriers [35], which would conceivably allow [^{18}F]VM4–037 to enter into the brain for imaging CA-IX

over-expression in brain tumors. Lastly, the high urinary bladder uptake of certain PET imaging agents limits the practical application of these agents for imaging tumors of the human prostate. The low retention of [^{18}F]VM4–037 in the urinary bladder may provide an opportunity to image CA-IX over-expression in nearby prostate tumors, a subset of which are known to over-express CA-IX. CA-IX targeting inhibitors utilizing a coumarin pharmacophore are not expected to strongly bind metalloproteases. ^{18}F-labeled CA-IX imaging agents utilizingbuild around this pharmacophore may result in reduced background organ uptake with improved CA-IX sensitivity [36]. Ultimately, a correlative pathology study comparing intratumoral CA-IX expression against [^{18}F]VM4037 uptake would help elucidate the tracer's ability to accurately target CA-IX overexpression.

Another concern arising out of the present study is the reduction of available radiotracer for tumor imaging by almost 50% due to the large retention in kidneys and liver. Further studies are needed to clarify whether the resulting reduced sensitivity is acceptable in patient imaging. Chemical modifications of the radiotracer may be needed to reduce the retention of the radiotracer in these organs and improve the sensitivity.

Comparison to other ^{18}F PET radiopharmaceuticals:

Table 4 lists whole body radiation dose and effective dose from [^{18}F]VM4–037 and from some other radiopharmaceuticals labeled with ^{18}F [25, 37–38]. We can observe that the radiation dose from [^{18}F]VM4–037 is similar to the radiation doses from other ^{18}F-based imaging agents. From a radiation dosimetry perspective, [^{18}F]VM4–037 is suitable for PET imaging in humans.

Conclusions:

The biodistribution of [^{18}F]VM4–037 is characterized by very high uptake in liver and kidneys, with little clearance of the activity during the 2.2 hr study period. The effective dose for a patient injected with the typical 370 MBq injected dose of [^{18}F]VM4–037 would be 10±0.5 mSv, and the kidney and liver doses would be 101±11 and 89±25 mGy respectively. Though the effective dose and the organ doses are within the limits considered as safe, the enhanced biodistribution of [^{18}F]VM4–037 in kidneys and liver may make the compound unsuitable for imaging CA-IX over-expression in those two organs in cancer patients. The clearance of [^{18}F]VM4–037 from plasma and muscle results in little residual background signal. This clearance profile may provide an opportunity to visualize metastatic disease or primary tumors in the lymph nodes, lung, and head and neck region. From a radiation dosimetry perspective, [^{18}F]VM4–037 is suitable for PET imaging in humans.

Acknowledgments

We wish to thank the nuclear medicine staff at the PET center including Donna Mosley for performing the PET/CT scans. We also wish to thank Mary Benetz and the staff from the Protocol Management Office for help with this research protocol. The help of the staff from Clinical Research Unit and Protocol Support Laboratory is gratefully acknowledged. The study was conducted at Fox Chase Cancer Center under a research contract with Siemens Molecular Imaging Inc. The study is registered in ClinicalTrials.gov with the identifier NCT00884520 and IND number 104438.

References:

1. Potter C, Harris AL (2004) Hypoxia inducible carbonic anhydrase IX, marker of tumour hypoxia, survival pathway and therapy target. Cell Cycle 3:164–167. [PubMed: 14712082]
2. Pastorek J, Pastorekova S (2004) Cancer-Related Carbonic Anhydrase Isozymes and Their Inhibition. CRC Press
3. Ivanov S, Liao SY, Ivanova A, et al. (2001) Expression of hypoxia-inducible cell-surface transmembrane carbonic anhydrases in human cancer. Am J Pathol 158:905–919. [PubMed: 11238039]
4. Winum JY, Rami M, Scozzafava A, Montero JL, Supuran C (2008) Carbonic anhydrase IX: a new druggable target for the design of antitumor agents. Med Res Rev 28:445–463. [PubMed: 17880011]
5. Pastorekova S, Parkkila S, Zavada J (2006) Tumor-associated carbonic anhydrases and their clinical significance. Adv Clin Chem 42:167–216. [PubMed: 17131627]
6. Potter CP, Harris AL (2003) Diagnostic, prognostic and therapeutic implications of carbonic anhydrases in cancer. Br J Cancer 89:2–7. [PubMed: 12838292]
7. Wykoff CC, Beasley NJ, Watson PH, et al. (2000) Hypoxia-inducible expression of tumor-associated carbonic anhydrases. Cancer Res 60:7075–7083. [PubMed: 11156414]
8. Chen L, Zhang Z, Kolb HC, Walsh JC, Zhang J, Guan Y (2012) (1)(8)F-HX4 hypoxia imaging with PET/CT in head and neck cancer: a comparison with (1)(8)F-FMISO. Nucl Med Commun 33:1096–1102. [PubMed: 22836736]
9. Ilie M, Mazure NM, Hofman V, et al. (2010) High levels of carbonic anhydrase IX in tumour tissue and plasma are biomarkers of poor prognostic in patients with non-small cell lung cancer. Br J Cancer 102:1627–1635. [PubMed: 20461082]
10. Jarvela S, Parkkila S, Bragge H, et al. (2008) Carbonic anhydrase IX in oligodendroglial brain tumors. BMC Cancer 8:1. [PubMed: 18173856]
11. Bui MH, Seligson D, Han KR, et al. (2003) Carbonic anhydrase IX is an independent predictor of survival in advanced renal clear cell carcinoma: implications for prognosis and therapy. Clin Cancer Res 9:802–811. [PubMed: 12576453]
12. Chia SK, Wykoff CC, Watson PH, et al. (2001) Prognostic significance of a novel hypoxia-regulated marker, carbonic anhydrase IX, in invasive breast carcinoma. J Clin Oncol 19:3660–3668. [PubMed: 11504747]
13. Loncaster JA, Harris AL, Davidson SE, et al. (2001) Carbonic anhydrase (CA IX) expression, a potential new intrinsic marker of hypoxia: correlations with tumor oxygen measurements and prognosis in locally advanced carcinoma of the cervix. Cancer Res 61:6394–6399. [PubMed: 11522632]
14. Kaanders JH, Wijffels KI, Marres HA, et al. (2002) Pimonidazole binding and tumor vascularity predict for treatment outcome in head and neck cancer. Cancer Res 62:7066–7074. [PubMed: 12460928]
15. Tanaka N, Kato H, Inose T, et al. (2008) Expression of carbonic anhydrase 9, a potential intrinsic marker of hypoxia, is associated with poor prognosis in oesophageal squamous cell carcinoma. Br J Cancer 99:1468–1475. [PubMed: 18841153]
16. Patard JJ, Fergelot P, Karakiewicz PI, et al. (2008) Low CAIX expression and absence of VHL gene mutation are associated with tumor aggressiveness and poor survival of clear cell renal cell carcinoma. Int J Cancer 123:395–400. [PubMed: 18464292]
17. McDonald PC, Winum JY, Supuran CT, Dedhar S (2012) Recent developments in targeting carbonic anhydrase IX for cancer therapeutics. Oncotarget 3:84–97. [PubMed: 22289741]
18. Divgi CR, Uzzo RG, Gatsonis C, et al. Positron Emission Tomography/Computed Tomography Identification of Clear Cell Renal Cell Carcinoma: Results From the REDECT Trial. J Clin Oncol 31:187–194. [PubMed: 23213092]
19. Neri D, Supuran CT (2011) Interfering with pH regulation in tumours as a therapeutic strategy. Nat Rev Drug Discov 10:767–777. [PubMed: 21921921]
20. Supuran CT (2008) Carbonic anhydrases: novel therapeutic applications for inhibitors and activators. Nat Rev Drug Discov 7:168–181. [PubMed: 18167490]

21. Kolb HC, Walsh JC, Dhanalakshmi K, et al. (2010) Development of Molecular Imaging Probes for Carbonic Anhydrase-IX Using Click Chemistry. US Patent US20100317842-A1. Issued Dec 16, 2010.
22. Stabin MG, Sparks RB, Crowe E (2005) OLINDA/EXM: the second-generation personal computer software for internal dose assessment in nuclear medicine. J Nucl Med 46:1023–1027. [PubMed: 15937315]
23. Doss M, Kolb HC, Zhang JJ, et al. (2012) Biodistribution and radiation dosimetry of the integrin marker ^{18}F-RGD-K5 determined from whole-body PET/CT in monkeys and humans. J Nucl Med 53:787–795. [PubMed: 22499613]
24. FDA (2010) Guidance for Industry and Researchers, The Radioactive Drug Research Committee: Human Research Without An Investigational New Drug Application.
25. Stabin M, Stubbs J, Toohey R (1996) Radiation dose estimates for radiopharmaceuticals, NUREG/CR-6345.
26. Hasannejad H, Takeda M, Taki K, et al. (2004) Interactions of human organic anion transporters with diuretics. J Pharmacol Exp Ther 308:1021–1029. [PubMed: 14610216]
27. Pastorekova S, Parkkila S, Pastorek J, Supuran CT (2004) Carbonic anhydrases: current state of the art, therapeutic applications and future prospects. J Enzyme Inhib Med Chem 19:199–229.
28. Pastorekova S, Casini A, Scozzafava A, Vullo D, Pastorek J, Supuran CT (2004) Carbonic anhydrase inhibitors: the first selective, membrane-impermeant inhibitors targeting the tumor-associated isozyme IX. Bioorg Med Chem Lett 14:869–873. [PubMed: 15012984]
29. Emara M, Turner AR, Allalunis-Turner J (2010) Hypoxic regulation of cytoglobin and neuroglobin expression in human normal and tumor tissues. Cancer Cell Int 10:33. [PubMed: 20828399]
30. Takacova M, Bartosova M, Skvarkova L, et al. (2013) Carbonic anhydrase IX is a clinically significant tissue and serum biomarker associated with renal cell carcinoma. Oncol Lett 5:191–197. [PubMed: 23255918]
31. Betof AS, Rabbani ZN, Hardee ME, et al. (2012) Carbonic anhydrase IX is a predictive marker of doxorubicin resistance in early-stage breast cancer independent of HER2 and TOP2A amplification. Br J Cancer 106:916–922. [PubMed: 22333602]
32. Kim SJ, Rabbani ZN, Dewhirst MW, et al. (2005) Expression of HIF-1alpha, CA IX, VEGF, and MMP-9 in surgically resected non-small cell lung cancer. Lung Cancer 49:325–335. [PubMed: 15935515]
33. Kim SJ, Rabbani ZN, Vollmer RT, et al. (2004) Carbonic anhydrase IX in early-stage non-small cell lung cancer. Clin Cancer Res 10:7925–7933. [PubMed: 15585626]
34. Li Y, Wang H, Oosterwijk E, et al. (2009) Expression and activity of carbonic anhydrase IX is associated with metabolic dysfunction in MDA-MB-231 breast cancer cells. Cancer Invest 27:613–623. [PubMed: 19367501]
35. Wolburg H, Noell S, Fallier-Becker P et al. (2012) The disturbed blood-brain barrier in human glioblastoma. Mol Aspects Med 33:579–589. [PubMed: 22387049]
36. McDonald PC, Winum JY, Supuran CT, Dedhar S (2012) Recent developments in targeting carbonic anhydrase IX for cancer therapeutics. Oncotarget 3:84–97. [PubMed: 22289741]
37. Doss M, Zhang JJ, Belanger MJ, et al. (2010) Biodistribution and radiation dosimetry of the hypoxia marker ^{18}F-HX4 in monkeys and humans determined by using whole-body PET/CT. Nucl Med Commun 31:1016–1024. [PubMed: 20948452]
38. Haubner R, Kuhnast B, Mang C, et al. (2004) [^{18}F]Galacto-RGD: synthesis, radiolabeling, metabolic stability, and radiation dose estimates. Bioconjug Chem 15:61–69. [PubMed: 14733584]

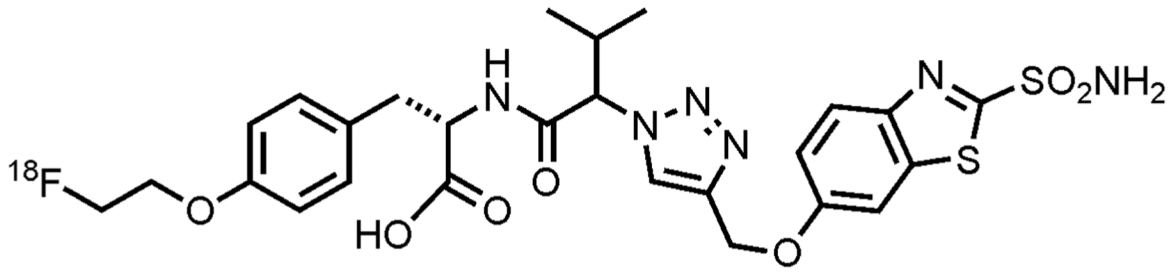

FIGURE 1.
Chemical structure of [^{18}F]VM4–037

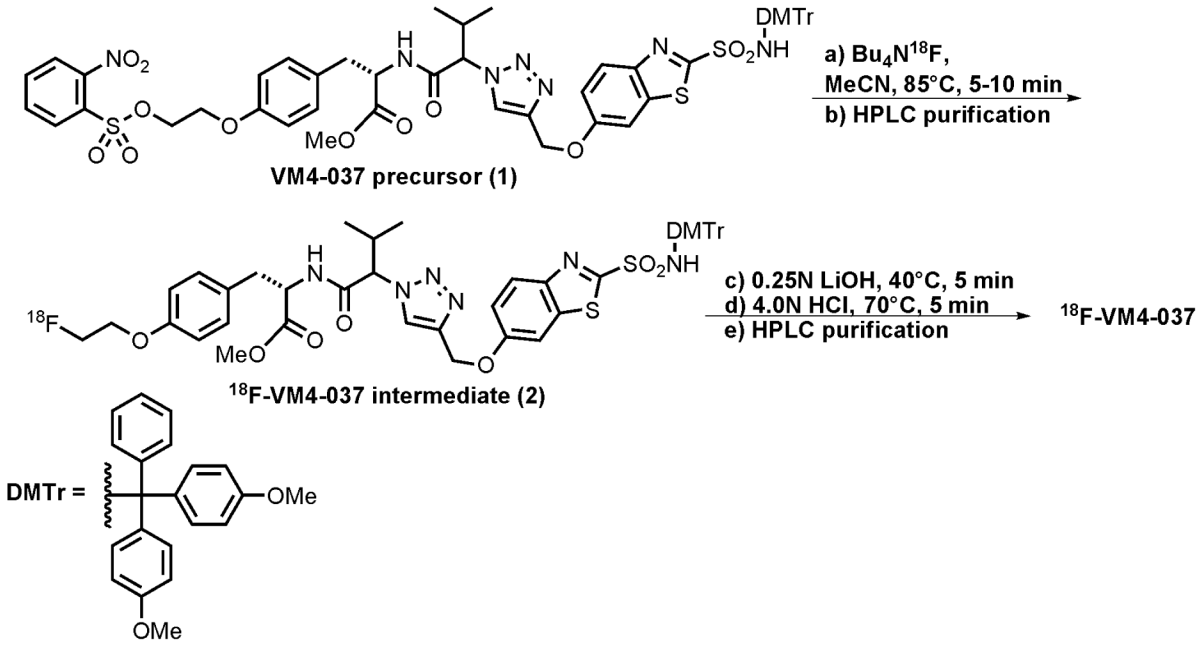

FIGURE 2.
Synthesis of [^{18}F]VM4–037

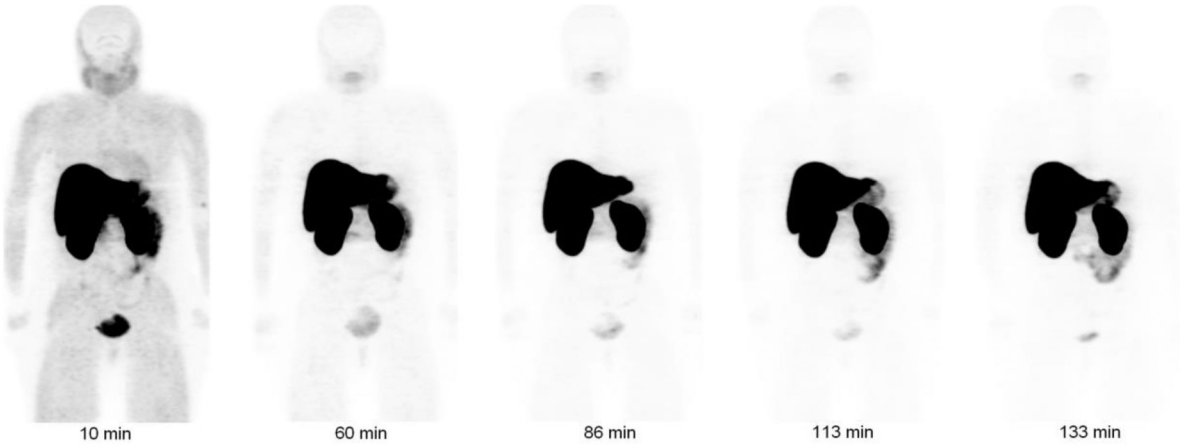

FIGURE 3.

Decay-corrected anterior maximum-intensity projections of PET at 10, 60, 86, 113, and 133 min (from left to right) after injection of [^{18}F]VM4–037 in a female subject. There is little clearance of activity through the renal system, and there is high uptake of activity in liver and kidneys.

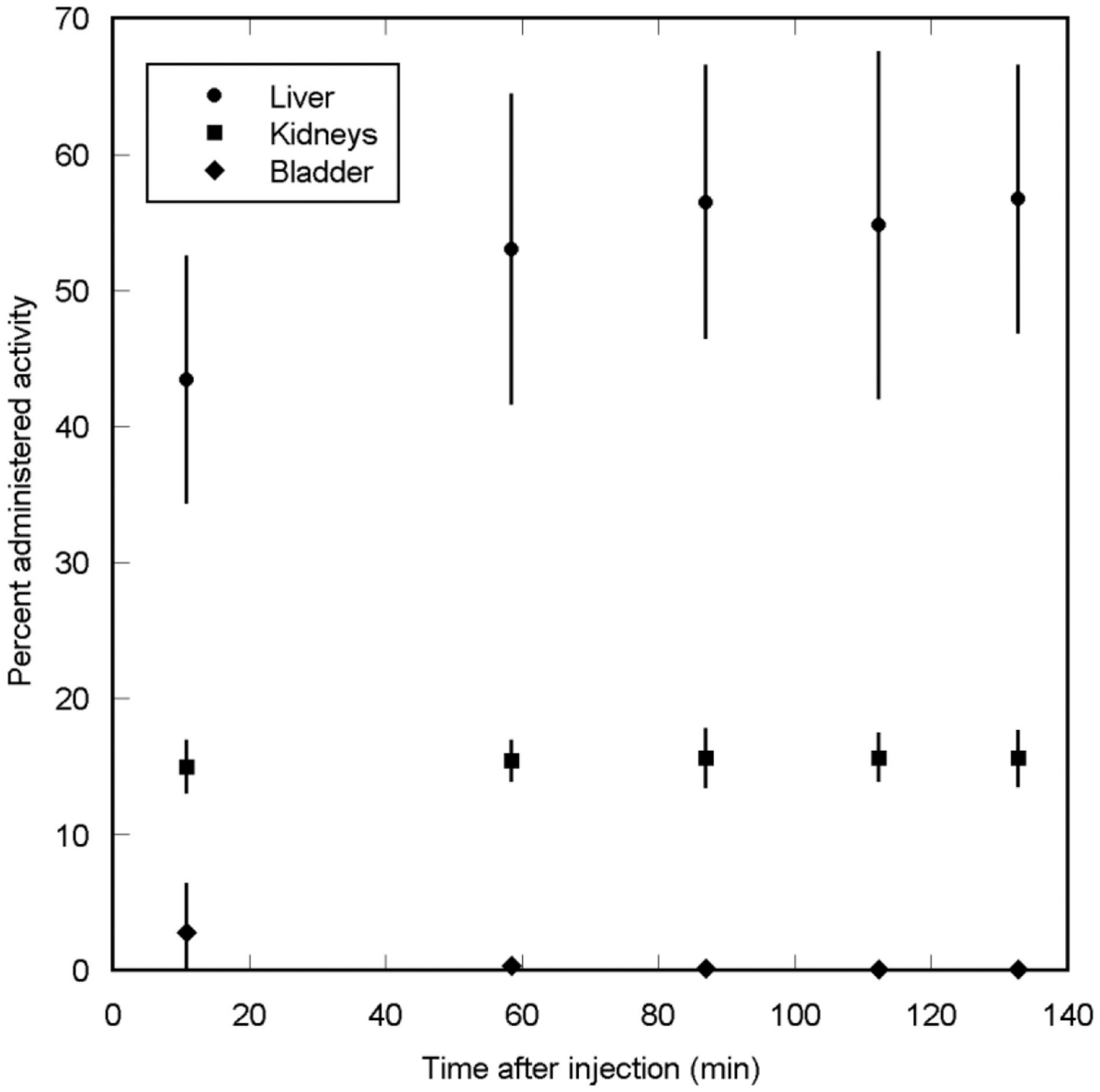

FIGURE 4.

Mean percent administered activity and SD for top 3 organs determined on basis of four [^{18}F]VM4–037 PET emission scans in human volunteers, as a function of time after injection. Little clearance of activity was observed in the organs.

TABLE 1.

Normalized number of disintegrations of Source Organs for Subjects injected with ^{18}F-VM4–037

	Normalized number of disintegrations
Organ	**(MBq-h/MBq administered)**
Brain	0.0061±0.0038
Gallbladder contents	0.010±0.009
Kidneys	0.42±0.05
Liver	1.92±0.56
Lower Large Intestine	0.013±0.011
Small Intestine	0.0055±0.0027
Upper Large Intestine	0.0068±0.0057
Urinary Bladder contents (1 h)	0.021±0.003
Urinary Bladder contents (4.8 h)	0.077±0.011
Remainder	0.50±0.31

Data are mean ± SD; n=4

TABLE 2.

Radiation dosimetry estimates per Unit Administered Activity for ^{18}F-VM4–037 for the Human Adult Male Phantom in 1- and 4.8-Hour Bladder-Voiding Models, Based on Human Biodistribution Data

	1 hr Void	4.8 hr Void
Organ	**(μGy/MBq)**	**(μGy/MBq)**
Kidneys	273±31	273±31
Liver	240±68	240±68
Gallbladder Wall	63±17	63±17
Adrenals	31±4.3	31±4.3
Pancreas	26±3.3	26±3.3
Upper Large Intestine Wall	17±1.8	17±1.8
Heart Wall	15±1.6	15±1.6
Spleen	14±1.4	14±1.5
Urinary Bladder Wall	14±2.2	41±5.7
Lungs	13±1.4	13±1.4
Small Intestine	13±1.1	13±1.1
Stomach Wall	13±0.8	13±0.8
Lower Large Intestine Wall	12±7.5	13±7.6
Red Marrow	9.3±0.6	9.4±0.5
Osteogenic Cells	8±1.5	8.1±1.5
Muscle	7.6±0.6	7.8±0.6
Ovaries	6.8±1.6	7.5±1.6
Uterus	6.5±1.5	8.1±1.6
Breasts	6.4±0.3	6.4±0.3
Thymus	6±0.7	6±0.7
Skin	4.7±0.6	4.7±0.6
Thyroid	3.2±1.4	3.2±1.4
Testes	2.9±1.5	3.4±1.5
Brain	1.7±0.7	1.7±0.7
Total Body	15±1.4	15±1.4
Effective Dose (μSv/MBq)	26±1	28±1

Data are mean ± SD; n=4

TABLE 3.

Organ doses for ^{18}F-VM4–037 and ^{18}F-FDG

_	^{18}F-VM4–037	^{18}F-FDG
Organ	**(μGy/MBq)**	**(μGy/MBq)**
Adrenals	32	13
Brain	1.7	19
Breasts	6.7	9
GallbladderWall	64	14
Heart_Wall	15	60
Kidneys	273	20
Liver	239	16
LLI_Wall	13	17
Lungs	13	17
Muscle	8.1	11
Osteogenic_Cells	8.6	12
Ovaries	7.9	17
Pancreas	27	26
Red_Marrow	10	13
Skin	5	8
Small_Intestine	13	14
Spleen	15	37
Stomach_Wall	23	13
Testes	4.1	13
Thymus	6.3	12
Thyroid	3.6	10
ULI_Wall	18	13
Urinary_Bladder_Wall	41	190
Uterus	8.6	23

TABLE 4.

Comparison of Dose per Unit Administered Activity Between ^{18}F-VM4–037 and Other ^{18}F Based Imaging Agents

	VM4–037		FDG	Galacto-RGD	HX4	
Bladder Voiding Interval	**1 hr**	**4.8 hr**	**4.8 hr**	**2 hr**	**1 hr**	**4.8 hr**
Total Body Dose (μGy/MBq)	15	15	11	5.34	8	10
Effective dose (μSv/MBq)	26	28	19	18.68	14	27